Journal of Ceramic Processing Research. Vol. 13, No. 4, pp. 432~436 (2012)

J O U R N A L O F
Ceramic Processing Research

Preparation and characterization of $M_3V_2O_8$ (M = Ba, Ca) nanoparticles by a MAS method

Chang Sung Lim*
Department of Advanced Materials Science & Engineering, Hanseo University, Seosan 356-706, Korea

$Ba_3V_2O_8$ and $Ca_3V_2O_8$ nanoparticles were synthesized successfully using a MAS (microwave-assisted solvothermal) method followed by further heat-treatment. Well-crystallized $Ba_3V_2O_8$ and $Ca_3V_2O_8$ nanoparticles were formed after heat-treatment at 600 °C for 3 h showing a fine and homogeneous morphology with particle sizes of 50-150 nm. The synthesized $Ba_3V_2O_8$ and $Ca_3V_2O_8$ nanoparticles were characterized by X-ray diffraction, Fourier transform infrared spectroscopy, scanning electron microscopy and transmission electron microscopy. The optical properties were investigated by photoluminescence emission and Raman spectroscopy.

Key words: $Ba_3V_2O_8$, $Ca_3V_2O_8$, MAS method, Nanoparticles, Luminescence, Raman spectroscopy.

Introduction

Microwave frustrated materials have recently attracted much interest, both theoretical and experimentally. Among various frustrated materials. metal orthovanadates have attracted considerable attention for potential applications in photoluminescence, IR-laser, light-emitting diode, photocatalyst, ferroelectric and microwave devices [1-3]. The magnetic ions M^{2+} form the so-called Kagome ladder, the MO^6 octahedra are located in zigzag layers separated by nonmagnetic ions V^{5+3}. The broadband emission in the visible light range is effective to obtain a good color rending property for lighting devices. To enhance the applications of $Ba_3V_2O_8$ and $Ca_3V_2O_8$, several processes have been developed over the past decade prepared by a range of processes, such as a solid-state reaction [4, 5], a solution phase metathetic method [6], a sol-gel method [7], a solid-state metathesis approach [8], a mechano-chemical method [9] and a floating zone technique [10].

Microwave energy is delivered to the surface of the material by radiant and/or convection heating, which is transferred to the bulk of the material via conduction with an electromagnetic field [11]. A hydrothermal process is an efficient low temperature method which allows the formation of particles with a high degree of crystallinity and easy dispersion in an aqueous medium. The use of microwave energy in a hydrothermal system promotes the development of a rapid heating to the required temperature with rapid rates of crystallization [12, 13]. Recently, MAS (microwave-assisted solvothermal) processes [14, 15] have been reported the simple use in preparing nanocrystalline particles of metal tungstates with unique and enhanced properties. A MAS process using a solvent of ethylene glycol is a convenient process that provides a high-qualified yield with a cost-effective method in short time periods.

Ethylene glycol, as a polar solvent with a boiling point of 197 °C, is a good candidate for a MAS process. When the solvent is ethylene glycol, the reactions proceed in a sealed pressure autoclave at temperatures at the boiling point of the ethylene glycol. The microwave radiation is supplied to the ethylene glycol, so that the components dissolving in the ethylene glycol are capable of coupling with radiation. When a large amount of microwave radiation is applied into the ethylene glycol under a high sealed pressure, the charged particles are vibrated in the electric field interdependently. Therefore, it is possible to achieve rapid and uniform heating of microwave dielectric materials. MAS reactions provide a convenient route for the synthesis of $Ba_3V_2O_8$ and $Ca_3V_2O_8$ particles, which were obtained in the form of loosely connected nano-sized particles at considerably lower temperatures with a high pressure than those usually employed for their synthesis.

In the present study, the $Ba_3V_2O_8$ and $Ca_3V_2O_8$ nanoparticles were synthesized using a MAS method. The characteristics of the synthesized $Ba_3V_2O_8$ and $Ca_3V_2O_8$ nanoparticles are discussed in detail based on the MAS reaction in ethylene glycol under a high sealed pressure. The synthesized $Ba_3V_2O_8$ and $Ca_3V_2O_8$ nanoparticles were characterized by X-ray diffraction (XRD), Fourier transform infrared spectroscopy (FTIR), scanning electron microscopy (SEM) and transmission electron microscopy (TEM). The optical properties were examined by photoluminescence (PL) emission and Raman spectroscopy.

*Corresponding author:
Tel : +82-41-660-1445
Fax: +82-41-660-1445
E-mail: cslim@hanseo.ac.kr

Experimental

Fig. 1 shows a flow chart for the synthesis of $Ba_3V_2O_8$ and $Ca_3V_2O_8$ nanoparticles by a MAS process. $BaCl_2{\cdot}2H_2O$, $CaCl_2$, Na_3VO_4 and ethylene glycol of analytic reagent grade (Aldrich) were used to prepare the $Ba_3V_2O_8$ and $Ca_3V_2O_8$ compounds. Each of 0.012 mol $BaCl_2{\cdot}2H_2O$ and 0.008 mol Na_3VO_4 for $Ba_3V_2O_8$ was dissolved in 30 ml ethylene glycol. In the same way, each of 0.012 mol $CaCl_2$ and 0.008 mol Na_3VO_4 for $Ba_3V_2O_8$ was dissolved in 30 ml ethylene glycol. The solutions were mixed and adjusted to a pH 9.5 using NaOH. The aqueous solution was stirred at room temperature. In the sequence, the mixture was transferred into a Teflon-lined digestion vessel of 120 ml capacity. The Teflon vessel was placed into a MAS oven (2.45 GHz, maximum power of 800 W). The MAS conditions were kept at 197 °C for 23 minutes. After the MAS process, the oven was cooled to room temperature. The resulting solutions were treated with ultrasonic radiation and washed many times with distilled hot water. The white precipitates were collected and dried at 100 °C in a dry oven. The final products were heat-treated at 600 °C for 3 h.

The existing phases of the $Ba_3V_2O_8$ and $Ca_3V_2O_8$ particles after the MAS process followed by further heat-treatment were identified by XRD (CuK_α, Rigaku D/MAX 2200, Japan). FTIR (Nicolet IR 200, Thermo Electron Corporation, USA) was used to examine the absorption behavior of the synthesized $Ba_3V_2O_8$ and $Ca_3V_2O_8$ particles over the frequency range, 400 to 4000 cm^{-1}. The microstructure, particle morphology and qualitative compositions of the $Ba_3V_2O_8$ and $Ca_3V_2O_8$ particles were observed by SEM (JSM-5600, JEOL, Japan) and TEM (JEM 2000-FX, 250 kV, Japan). The PL spectra were recorded using a spectrophotometer (Perkin Elmer LS55, UK) at room temperature. Raman spectroscopy measurements were performed using a LabRam HR (Jobin-Yvon, France). The 514.5 nm line of an Ar-ion laser was used as the excitation source, the power was kept at 0.5 mW on the samples.

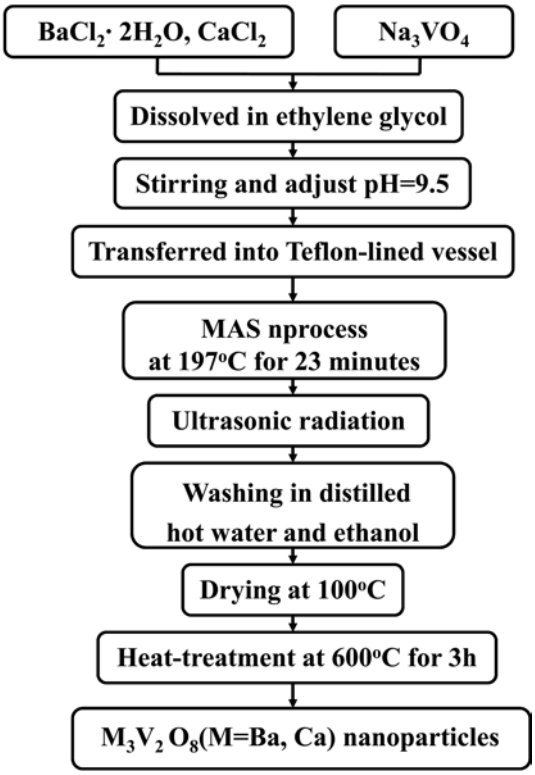

Fig. 1. Flow chart for the synthesis of $Ba_3V_2O_8$ and $Ca_3V_2O_8$ nanoparticles by the MAS process.

Results and discussion

Fig. 2 shows XRD patterns of the synthesized (a) $Ba_3V_2O_8$ and (b) $Ca_3V_2O_8$ nanoparticles. All the observed diffraction peaks could be assigned to the trigonal phases, which is in good agreement with the crystallographic data of $Ba_3V_2O_8$ (JCPDS: 71-2060, space group *R-3m*) and $Ca_3V_2O_8$ (JCPDS: 46-756, space group *R3c*) [8]. These suggest that MAS synthesis is suitable for the growth of $Ba_3V_2O_8$ and $Ca_3V_2O_8$ crystallites with the strongest major intensity peaks from the (015), (110) and (205) planes for $Ba_3V_2O_8$ in Fig. 2(a), and (210) and (220) planes for $Ca_3V_2O_8$ in Fig. 2(b) with some preferred orientation, respectively.

Fig. 3 shows FT-IR spectra of the (a) $Ba_3V_2O_8$ and (b) $Ca_3V_2O_8$ nanoparticles synthesized by the microwave solvothermal process followed by further heat-treatment at 600 °C for 3 h in the wavenumber range, 480-4000 cm^{-1}.

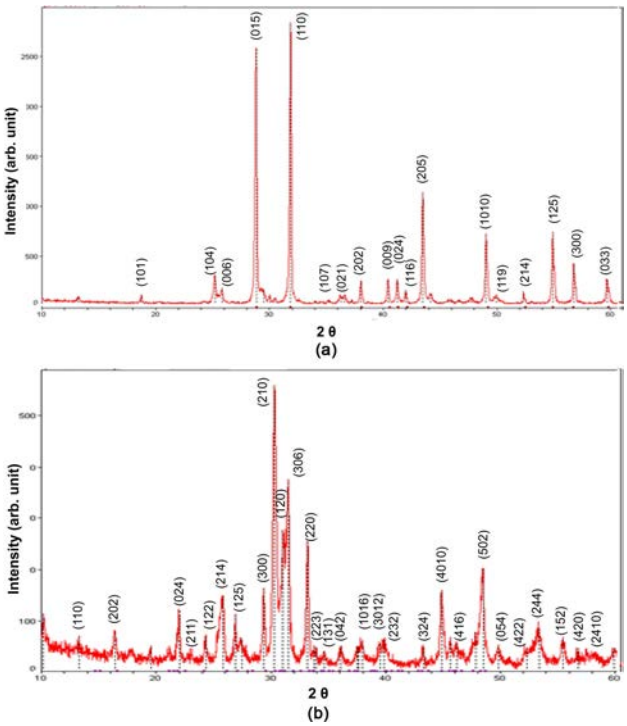

Fig. 2. XRD patterns of the synthesized (a) $Ba_3V_2O_8$ (a) and (b) $Ca_3V_2O_8$ nanoparticles.

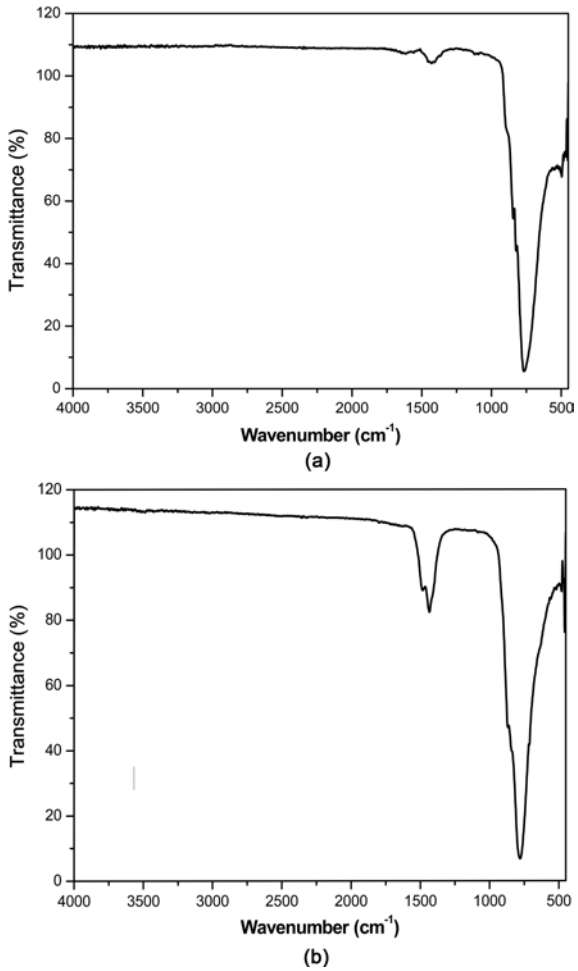

Fig. 3. FT-IR spectra of the synthesized (a) $Ba_3V_2O_8$ and (b) $Ca_3V_2O_8$ nanoparticles.

The large isolated absorbable peak around 820 cm^{-1} reveals typical characteristics of a strong V-O stretching in the $[VO_4]^{3-}$. The strong V-O stretching peaks are contributed to the uniform regular $[VO_4]^{3-}$ tetrahedra of the metal orthovanadates. The band at 1450 cm^{-1} is assumed that the samples prepared contain a small amount of surface-adsorbed water and alcohol.

Fig. 4 shows a SEM image (a) and a TEM image (b) of the synthesized $Ba_3V_2O_8$ nanoparticles. The SEM image of $Ba_3V_2O_8$ in Fig. 4(a) shows a well-defined and homogeneous morphology, while the TEM image of $Ba_3V_2O_8$ in Fig. 4(b) shows the particle sizes of 50-150 nm. Fig. 5 shows a SEM image (a) and a TEM image (b) of the synthesized $Ca_3V_2O_8$ nanoparticles. The SEM image of $Ca_3V_2O_8$ in Fig. 5(a) shows a well-defined and homogeneous morphology, while the TEM image of $Ca_3V_2O_8$ in Fig. 5(b) shows the particle sizes of 50-150 nm. The MAS synthesis proceeds the reaction of $BaCl_2 \cdot 2H_2O + Na_3VO_4$ and $CaCl_2 + Na_3VO_4$ in a hot ethylene glycol solution as a polar solvent with a boiling point of 197 °C. The MAS process occurs in accordance with the reaction: $3BaCl_2 \cdot 2H_2O + 2Na_3VO_4 \rightarrow Ba_3V_2O_8 + 6NaCl + 6H_2$

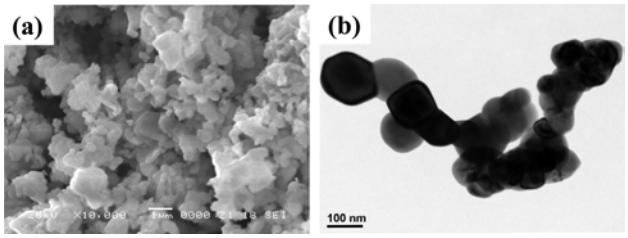

Fig. 4. A SEM image (a) and a TEM image (b) of the synthesized $Ba_3V_2O_8$ nanoparticles.

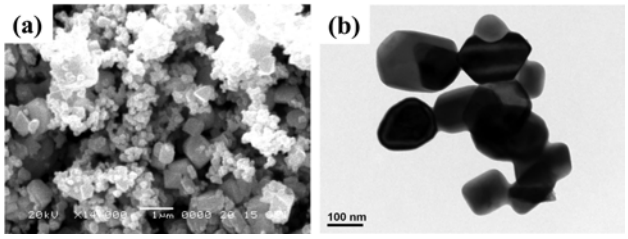

Fig. 5. A SEM image (a) and a (b) TEM image (b) of the synthesized the $Ca_3V_2O_8$ nanoparticles.

O and b$3CaCl_2 + 2Na_3VO_4$ $Ca_3V_2O_8 + 6NaCl$.

When the microwave radiation is supplied to the ethylene glycol under a sealed pressure at the boiling point, the components dissolving in the ethylene glycol are charged and vibrated in electric field interdependently. The MAS process is adjusted to heat the metal orthovanadates uniformly resulting in fine particles with a controlled morphology, and to fabricate the product in a green manner without the generation of solvent waste. The MAS reaction involves the exchange of atomic/ionic species, where the driving force is the exothermic reaction in ethylene glycol accompanying the formation of NaCl with a high lattice energy. The exothermic reaction occurs so rapidly that the temperature and the pressure of the ethylene glycol increases so quickly that the reaction products are essentially heated up. The MAS reactions provide a convenient and fast route for the synthesis of $Ba_3V_2O_8$ and $Ca_3V_2O_8$ nanoparticles at considerably lower temperatures with a high pressure than those usually employed for their synthesis. The well-defined $Ba_3V_2O_8$ and $Ca_3V_2O_8$ nanoparticle features synthesized by the MAS process have a control over the morphology of the fine particles, and can be used for technological applications.

Fig. 6 shows PL emission spectra of the synthesized (a) $Ba_3V_2O_8$ and (b) $Ca_3V_2O_8$ nanoparticles excited at 250 nm at room temperature. With excitation at 250 nm, $Ba_3V_2O_8$ particles in Fig. 6(a) exhibit major PL emissions in the blue wavelength range of 390-430 nm. The emission spectra of three narrow shoulders at approximately 490, 510 and 530 nm are considered to form by defect structures. With excitation at 250 nm, $Ca_3V_2O_8$ particles in Fig. 6(b) exhibit PL emission in the blue wavelength range of 390-430 nm. The emission spectra of four narrow shoulders at approximately 490, 510, 530 and 540 nm are considered

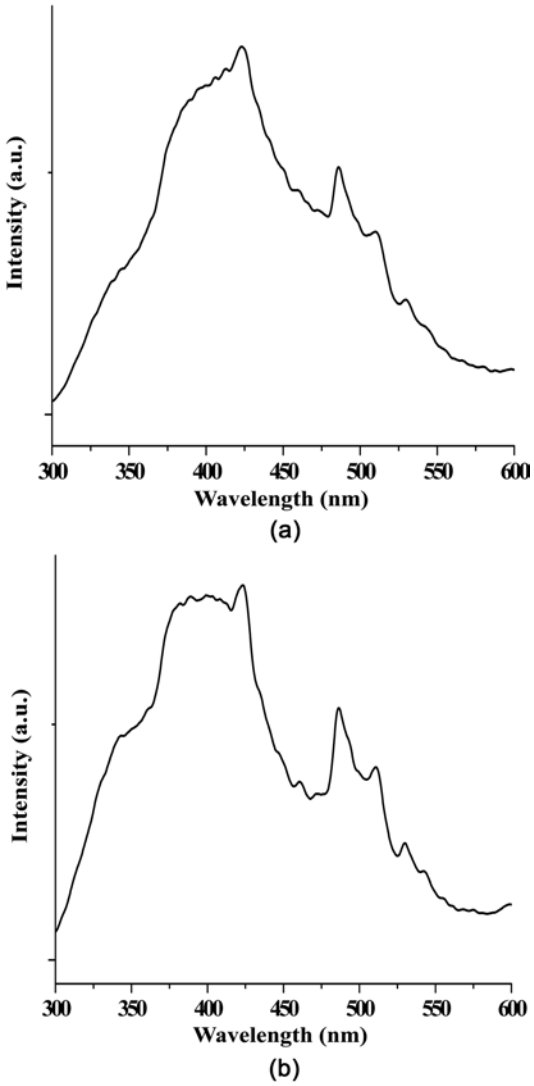

Fig. 6. PL emission spectra of the synthesized (a) $Ba_3V_2O_8$ and (b) $Ca_3V_2O_8$ nanoparticles excited at 250 nm at room temperature.

to form by defect structures. The emission spectra of metal orthovanadates are due mainly to charge-transfer transitions within the $[VO_4]^{3-}$ complex. The explanation of the narrow shoulders in Fig. 6(a, b) is proposed considering the Jahn-Teller splitting effect [16, 17] on excited states of $[VO_4]^{3-}$ and anions in the $Ba_3V_2O_8$ and $Ca_3V_2O_8$. This is similar to that reported by Zhan et al. [18]. The Jahn-Teller splitting effect essentially determines the emission shape of the $Ba_3V_2O_8$ and $Ca_3V_2O_8$ particles. The additional emission bands can be interpreted by the existence of Frenkel defect structures (oxygen ions shifted to the inter-position with the simultaneous creation of vacancies) in the surface layers of the $Ba_3V_2O_8$ and $Ca_3V_2O_8$ particles [19, 20].

Fig. 7 shows Raman spectra of the synthesized (a) $Ba_3V_2O_8$ and (b) $Ca_3V_2O_8$ nanoparticles excited by the 514.5 nm line of an Ar-ion laser at 0.5 mW on the samples. The vibration modes in the Raman spectra of the $Ba_3V_2O_8$ and $Ca_3V_2O_8$ nanoparticles are classified into two groups, internal and external. The internal

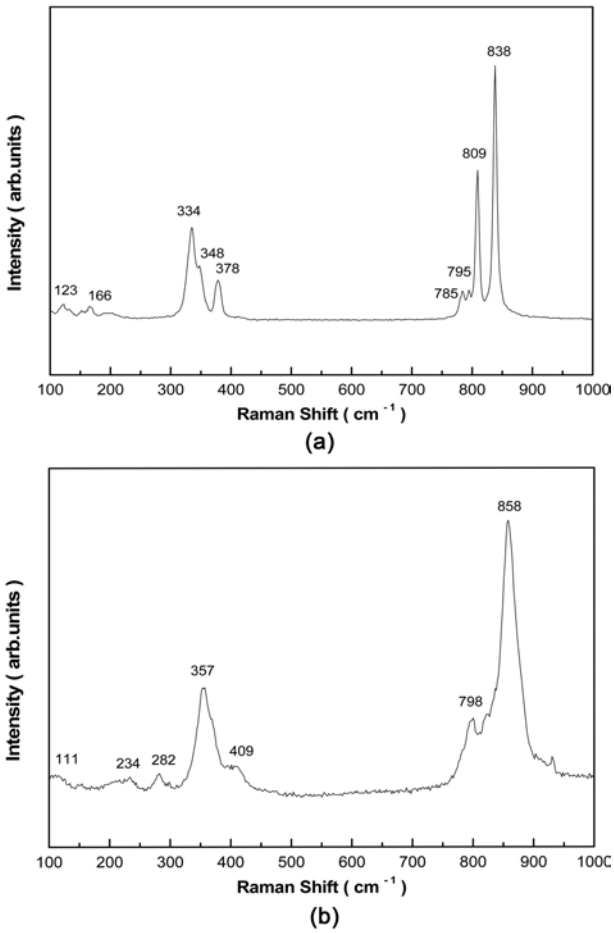

Fig. 7. Raman spectra of the synthesized (a) $Ba_3V_2O_8$ and (b) $Ca_3V_2O_8$ nanoparticles excited by the 514.5 nm line of an Ar-ion laser at 0.5 mW on the samples.

vibrations are related to the $[VO_4]^{3-}$ molecular group with a stationary mass center. The external vibrations or lattice phonons are associated with the motion of the Ba^{2+} and Ca^{2+} cations and rigid molecular units [21]. The Raman modes for the $Ba_3V_2O_8$ particles were detected at 838, 809, 795, 378, 334 and 334 cm^{-1}, the free rotation mode was detected at 166 cm^{-1} and the external mode was localized at 123 cm^{-1}. The Raman modes for the $Ca_3V_2O_8$ particles were detected at 858, 798, 409 and 357 cm^{-1}, the free rotation modes were detected at 282-234 cm^{-1} and the external mode was localized at 111 cm^{-1}. The well-resolved sharp peaks for the $Ba_3V_2O_8$ and $Ca_3V_2O_8$ nanoparticles indicate that the synthesized particles are highly crystallized.

Conclusions

$Ba_3V_2O_8$ and $Ca_3V_2O_8$ nanoparticles were synthesized successfully by a MAS method in a hot ethylene glycol solution as a polar solvent. Well-crystallized $Ba_3V_2O_8$ and $Ca_3V_2O_8$ nanoparticles were formed after heat-treatment at 600 °C for 3 h showing a fine and homogeneous morphology with particle sizes of 50-150 nm. With excitation at 250 nm, the $Ba_3V_2O_8$ and

$Ca_3V_2O_8$ exhibited major PL emissions in the blue wavelength range of 390-430 nm. The internal Raman modes for the $Ba_3V_2O_8$ particles were detected at 838, 809, 795, 378, 334 and 334 cm^{-1}, the free rotation mode was detected at 166 cm^{-1} and the external mode was localized at 123 cm^{-1}. The internal Raman modes for the $Ca_3V_2O_8$ particles were detected at 858, 798, 409 and 357 cm^{-1}, the free rotation modes were detected at 282-234 cm^{-1} and the external mode was localized at 111 cm^{-1}. The well-resolved sharp peaks for the $Ba_3V_2O_8$ and $Ca_3V_2O_8$ nanoparticles indicate that the synthesized particles are highly crystallized.

Acknowledgement

This study was supported by Basic Science Research Program through the National Research Foundation of Korea (NRF) funded by the Ministry of Education, Science and Technology (2011-0026911).

References

1. T. Nakajima, M. Isobe, T. Tsuchiya, Y. Ueda, T. Kumagai, J. Luminescence 129 (2009) 1598-1601.
2. F. Yen, R.P. Chaudhury, E. Galstyan, B. Lorenz, Y.Q. Wang, Y.Y. Sun, C.W. Chu, Physica B 403 (2008) 1487-1489.
3. N. Rogado, G. Lawes, D.A. Huse, A.P. Ramirez, R.J. Cava, Solid State Comm. 124 (2002) 229-233.
4. D. Wang, Z. Zou, J. Ye, Res. Chem. Intermed. 31 (2005) 433-439.
5. M. Kurzawa, A. Blonska-Tabero, J. Therm. Anal. Calorim. 77 (2004) 17-24.
6. P. Parhi, V. Manivannan, Mat. Res. Bull. 43 (2008) 2966-2973.
7. S.S. Kim, H. Ikuta, M. Wakihara, Solid State Ionics 139 (2001) 57-65.
8. P. Parhi, V. Manivannan, S. Kohli, P. Mccurdy, Bull. Mater. Sci. 31 (2008) 885-890.
9. V. Manivannan, P. Parhi, J. Howard, J. Cry. Growth 310 (2008) 2793-2799.
10. R. Szymczak, M. Baran, J. Fink-Finowicki, B. Krzymanska, P. Aleshkevych, H. Szymczak, S.N. Barilo, G.L. Bychkov, S.V. Shiryaev, J. Non-Crystalline Solids 354 (2008) 4186-4188.
11. S. Das, A.K. Mukhopadhyay, S. Datta, D. Basu, Bull. Mater. Sci. 32 (2009) 1-13.
12. K.P.F. Siqueira, R.L. Moreira, M. Valadares, A. Dias, J. Mat. Sci. 45 (2010) 6083-6093.
13. J.C. Sczancoski, L.S. Cavalcante, M.R. Joya, J.a. Varela, P.S. Pizani, E. Longo, Chemical Eng. J. 140 (2008) 632-637.
14. J. Bi, L. Wu, Z. Li, Z. Ding, X. Wang, X. Fu, J. Alloys & Comp. 480 92009) 684-688.
15. T. Thongtem, A. Phuruangrant, S. Thongtom, Curr. Appl. Phy. 8 (2008) 189-197.
16. Y. Toyozawa, M. Inoue, J. Phys. Soc. Jpn. 21 (1966) 1663-1679.
17. E.G. Reut, Izv. Akad. Nauk SSSR, Ser. Fiz. 43 (1979) 1186-1193.
18. Y. Zhang, N.A.W. Holzwarth, R.T. Williams, Phys. Rev. B 57 (1998) 12738-12750.
19. J. Van Tol, J.H. Van Der Waals, Mol. Phys. 88 (1996) 803-820.
20. V.B. Mikhailik, H. Kraus, D. Wahl, M.S. Mykhaylyk, Phys. Status Solid B 242 (2005) R17-R19.
21. T.T. Basiev, A.A. Sobol, P.G. Zverev, L.I. Ivleva, V.V. Osiko, R.C. Powell, Opt. Mat. 11 (1999) 307-314.